Low Frequency influence on degradation of commercial Li-ion battery

(article starts on next page)

Low Frequency influence on degradation of commercial Li-ion battery

Kristian Frenander [a,b,*], Torbjörn Thiringer [a]

[a] Department of Electrical Engineering, Chalmers University of Technology, SE-412 96, Gothenburg, Sweden
[b] Volvo Car Corporation, SE-405 31, Gothenburg, Sweden

ARTICLE INFO

ABSTRACT

The Tesla model 3 has rapidly become one of the most popular electric vehicles (EV), being the best selling EV in 2020 and the second best selling in 2021. In this paper the ageing implications of varying time scales in usage of the battery are investigated for the 2170 cells used in the Tesla model 3. It is shown that dynamic usage in the range of approximately 0.01 to 0.1 Hz has a statistically significant impact on ageing, while dynamic usage in range 0.1 to 1 Hz does not show significant impact on ageing. Furthermore the individual electrode ageing is investigated by non-invasive electrochemical techniques, revealing the profound impact on ageing from Si addition to the negative electrode, where it is shown that substantial part of the ageing comes from loss of Si in the negative electrode.

1. Introduction

In recent years the push to increase electrification of the vehicle fleets across the world has gained momentum and the market shares have been increasingly rapidly in many countries. During this period the Battery Electric Vehicle (BEV) with a Lithium-ion Battery (LiB) has matured into the most popular variant of electrified vehicle (EV). This process has been enabled by rapid development of the LiBs used in the automotive industry, but since the battery is still the largest and most expensive component in a BEV understanding their behaviour and optimising their utilisation remains an important topic for industry and research alike.

This development has lead to increased interest in many aspects of the LiB, from improving energy density and performance to prolonging service life. One of the chemistries that has been generating interest is Silicon negative electrodes. This is due to the high capacity of Si as negative electrode material, as it alloys with Li in a more efficient way that standard intercalation materials, yielding $4212 \, \text{mA h g}^{-1}$ [1] theoretical capacity and a practical capacity around $3579 \, \text{mA h g}^{-1}$ for Li15Si4 [2–4]. This is a very tangible improvement compared to $372 \, \text{mA h g}^{-1}$ for graphite [5]. Moreover, silicon's attractiveness is increased by the material's abundance and non-toxicity [1]. However, large volumetric contraction and expansion [6] causes durability issues with unstable SEI, particle pulverisation and morphology changes [7] during alloying and dealloying. This rapid degradation of pure Si electrodes have hampered their industrialisation. In recent years the development of Silicon based electrodes has been rapid [8] and these drawbacks have been partially overcome, for instance by producing composite electrodes where

the silicon works as a dopant to graphite electrode to add capacity. This technique is now used widely in commercial cells available off the shelf, but still only a relatively small body of literature is available concerning its durability effects, especially when considering an NCA positive electrode.

Liu et al. [9] have reported degradation data for cells comprising an NCA positive electrode and a Si-Gr composite negative electrode with static current and found little influence of the discharge current, but it should be noted that their investigation was limited to non-dynamic tests. Teichert et al. [10] investigated the ageing challenges for Ni-rich positive electrodes, specifically focusing on the ageing mechanisms occurring in the cells, with the investigation limited to the positive electrode. Farmakis et al. [11] performed interesting investigations comparing the ageing behaviour of cells with an NCA positive electrode versus pure Si or pure graphite, using standard galvanostatic cycling, and were able to conclude that a Si negative electrode was detrimental to battery lifetime. However they did not extend their investigation to include mixed materials.

Jossen and co-workers [12], have found that ageing implications are not homogeneous for the two materials making up the composite electrode. Instead it can be seen that the graphite is losing capacity less rapidly than the Si, leading to a shift of the OCV of the negative electrode, and corresponding change in cell OCV. They have also investigated how the fraction of Si added to the negative electrode affects the durability and found a negative correlation between the amount of Si and the capacity retention [13] and performed studies in the calendar ageing behaviour and reversibility of capacity loss of cells with

Si-Gr composite electrodes [14]. Profatilova et al. [15] investigated the influence of porosity on the durability for Si-Gr electrodes and found that the influence of porosity on transport properties led to significantly different ageing when porosity decreased. Important to note is that these studies did not extended their scope beyond constant current cycles.

Interesting investigations of the influence of drive cycles on battery ageing was conducted by Baure and Dubarry [16] who compared drive cycles used in certification to real driving data, as well as Keil and Jossen [17] who investigated the effects of regenerative braking during dynamic driving, and different SOC levels, for non-parameterised discharge and drive cycles. Schmalstieg et al. [18] implemented parameterised customer profiles to investigate effects of waiting times and other parts of the usage behaviour, for constant current discharge cycling. Further important work was conducted by Peterson et al. [19] investigating realistic usage conditions for a Vehicle-to-Grid (V2G) user, including realistic drive cycles and investigating different customer profiles, however not including a discharge pattern that could be reduced to a small number of governing parameters. Bessmann et al. [20] implemented discharge profiles combining a DC discharge and AC harmonics, for frequency ranges above 1 Hz.

Despite the valuable and interesting research being published in the field, to the best of the authors' knowledge there are no papers where representative parameterisable discharge patterns are developed or used to investigate the effect of the discharge dynamics on the cell ageing. In order to fill this research gap, a novel test method for investigating the sensitivity to the dynamic pulses of driving is suggested in this paper, making standardised dynamic testing possible, allowing researchers to investigate ageing behaviour more akin to real world scenarios. This methodology can also be further expanded to investigate other usage parameters derived from real world driving and the highly variable nature of the current profiles that batteries are exposed to in EV applications.

Accordingly, the aim of this paper is to establish the influence on Lithium-ion battery ageing due to low frequency current pulses, with a specific focus on cells with silicon doped composite electrodes.

The key novel contributions of this article are

- Reporting of cycling data for cells with NCA positive electrode and Si-Gr negative electrode.
- A proposal of a parameterisable dynamic discharge pattern and demonstration of its feasibility when implemented in a battery testing equipment.
- Proof of the possibility to use the low-SOC hysteresis as tool for non-invasive ageing assessment in composite electrode cells.
- Demonstration of a correlation of ageing and pulse harmonics in the range of 10 to 100 mHz, while showing no correlation for frequencies in the range 100 to 1000 mHz.

2. Experimental

2.1. Cells and setup

The 2170 cells tested for this study are from a Tesla model 3 car to ensure it is production status cells. Samples were also taken from cells to build halfcells for electrode characterisation. Its chemistry is a mixed silicon and graphite negative electrode paired with a Nickel-Cobalt-Aluminium (NCA) positive electrode. Some further technical details are given in Table 1.

To investigate the influence of the typically stochastic discharge behaviour, a suitable dynamic discharge pattern is developed. The main interest of this study was to investigate the effect of different time scales on the ageing behaviour, since different drive patterns give rise to vastly different time scales of discharge, quite dissimilar from the idealised steady state currents typically used in laboratory ageing studies.

Table 1
Technical specifications of the Panasonic 2170 cell.

Parameter	Cell specifications
Manufacturer	Panasonic
Geometry	Cylindrical 2170
Chemistry	NCA/Si-Gr
Capacity	4.6 A h
Weight	68.45 g
Dimensions	21 mm × 70 mm
U_{max}	4.18 V
U_{min}	2.55 V
U_{nom}	3.6 V
Gravimetric energy density	242 W h kg^{-1}

Table 2
Tabular representation of reference performance test (RPT) as performed every 50 cycles of cycle life testing.

Measurement	Procedure	Comment
Capacity	CCCV Charge $I_{cutoff} = C/20$	Cut at U_{max}
Repeat x2	CC Discharge $I = C/3$	Cut at U_{min}
ICA	CC Charge $I = C/20$	Cut at U_{max}
	CC Discharge $I = C/20$	Cut at U_{min}
Impedance	CCCV Charge $I_{cutoff} = C/20$	Cut at U_{max}
	CC Discharge $I = C/3$ to 70%, 50%, 30% SOC	Break based on voltage corresponding to X% SOC
	10 s pulse $I_{pulse} = 1.3$ C	Max current on tester Charge and discharge

A cycling protocol was developed where the cell would undergo different discharge cycles with a maintained mean current of 1C to yield comparable results. This was achieved by applying a rectangular wave discharge current of 1.33C during three quarters of a repeating cycle, while resting the remaining quarter of the cycle, see Fig. 2 for clarification of the discharge profile. The total time of the repeating cycle is then varied to yield the different discharge protocols. As a reference cycle a standard 1C test was also performed.

The total time in the test matrix was varied to obtain a suitable distribution in the frequency domain by varying the total time according to $t_{total} = 2^N$ s where $N \in \{0, 1, \ldots, 8\}$, or from 1 s to 256 s with the frequency of the test defined as $f_{test} = 1/t_{total}$. This yields a frequency range from 4 mHz to 1 Hz. While the main purpose of the test design is to allow for direct comparison with standard 1C tests it can be interesting to note that the typical frequencies found in standard urban (Artemis urban) and highway (US06 and Artemis 130) drive cycles range from about 10 to 200 mHz with maximum occurrence around $\sim$ 25 mHz, identified using fast Fourier transform (FFT) on the speed trace of the cycles. Thus, the tested frequency range is not dissimilar to what could be expected from real world applications. All tests were performed with a minimum of two replicates in a temperature of 25 °C.

2.2. Reference test

All cells underwent regular checkups every 50 full cycle equivalents (FCE) where the discharge capacity was measured at $I_{dchg} = C/3$ current after performing a C/3 CCCV charging with $I_{cutoff} = C/20$ at U_{max}. This cycle was repeated twice and the average of the two values was utilised as capacity figure for that reference test.

After determining the capacity of the cell an incremental capacity sweep was done at $I_{ICA} = C/20$, sweeping both charge and discharge direction between U_{min} and U_{max}.

The final step of the reference test was a pulse test to measure resistance of the cell, run with 10 s pulses of $I_{pulse} = 1.3C$. The
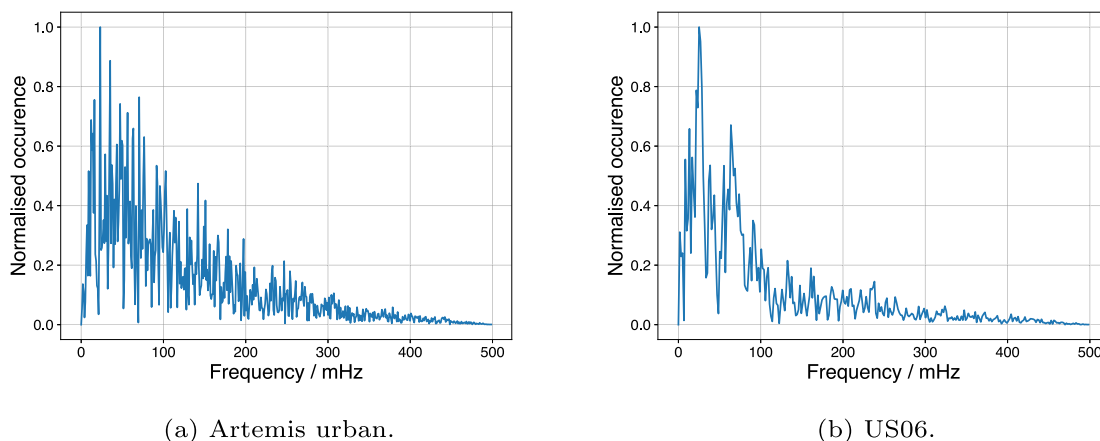
(a) Artemis urban.

(b) US06.

Fig. 1. Normalised frequency spectra from FFT on speed trace of two standard drive cycles, with (a) showing *Artemis Urban*, a drive cycle used to represent urban driving. Correspondingly in (b) the frequency spectrum from FFT on *US06*, a highway drive cycle, is depicted.
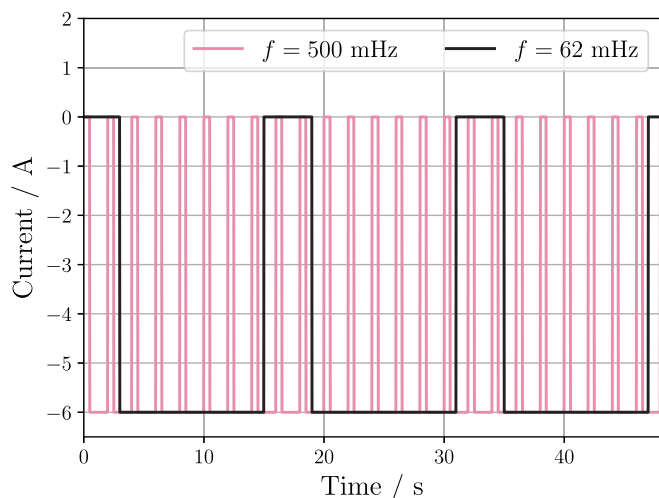

Fig. 2. Schematic visualisation of the pulse discharge pattern used in the study.

current level used in the pulse was set by the maximum current limit provided by the tester, see Section 2.4. The pulses were applied at three different SOC levels of 30, 50 and 70% with both charge and discharge pulses applied to the cell. See Table 2 for clarification and a tabular representation of reference test procedure.

On top of this basic checkup test a subset of the cells also underwent further tests to obtain a more complete characterisation. The additional tests were Intermittent Current Interruption (ICI) test and Electrochemical Impedance Spectroscopy. The ICI test procedure is described in [21]. In this study it was implemented with $I_{ICI} = C/20$ applied for 300 s and current interruptions of 5 s and the test was performed during every reference test.

The cells that performed regular ICI were also characterised using regular electrochemical impedance spectroscopy (EIS) sweeps. However due to requiring specific equipment (see Section 2.4) and lead time for the test, these tests were only performed every 300 FCE to reduce stoppages. The lead time was mainly due to conditioning, as the cells needed to be brought to 50% SOC level for the test and then fully equilibrated for 12 h before the test was performed. The EIS sweeps were run between 10 kHz and 10 mHz with 10 points per decade and a 10 mV perturbation applied.

2.3. Individual electrode analysis

To enable half cell analysis electrode materials were harvested from a fresh cell and reconstructed into half cells with a lithium metal counter electrode. These cells were assembled into pouch cells, using electrode discs with ⌀15 mm with a ⌀18 mm lithium metal counter electrode and a Whatman 260 μm separator.

These single electrode cells were cycled using $C/10$ current to obtain reference OCV curve for electrodes. The Si-Gr electrode was cycled between 0.002 V and 1.5 V and the NCA electrode was cycled between 3 V and 4.35 V to obtain full voltage curves.

2.4. Test equipment

All cycling testing and the reference tests were performed using a Neware BTS4000 5 V battery testing system with a maximum current of $I_{max,tester} = 6$ A. The EIS measurements were performed on a Gamry reference 3000 tester with a frequency range of 1 mHz to 300 kHz.

3. Results and discussion

The capacity fade results of the tests are shown in Fig. 3. From this figure it can be noted that the spread in results is significant even between cells performing exactly the same test. This type of behaviour has been investigated for cells connected in modules or packs [22,23] which experience slightly different conditions during ageing, but has not been investigated for cells performing identical tests. Despite the spread, there is a trend that can be noted which is that the capacity of the cells that are subjected to higher frequency pulses is decaying more rapidly than those performing pulses with lower frequency. This trend, and the noise in the data, can be seen more clearly from Fig. 5 where the average energy throughput through the cells before reaching end of life is plotted versus the frequency applied in the test. As can be seen from the box plot, the data is noisy, but with a trend towards higher energy throughput before reaching end of life for the cells cycled with lower frequency pulses. This would indicate that more stationary loads on the battery, corresponding to less dynamic driving with more constant speed, would be beneficial for the mileage one can get out of an electric vehicle before it reaches end of life. It can also be noted that there is significant capacity recuperation in some tests, which occurs when testing is temporarily halted to perform EIS tests, see Section 2.2, as this led to a rest period for all cells before the tests were restarted. This behaviour has previously been reported in several previous works [24–26] and is believed to be related to negative electrode overhang storing excess capacity of lithium ions.
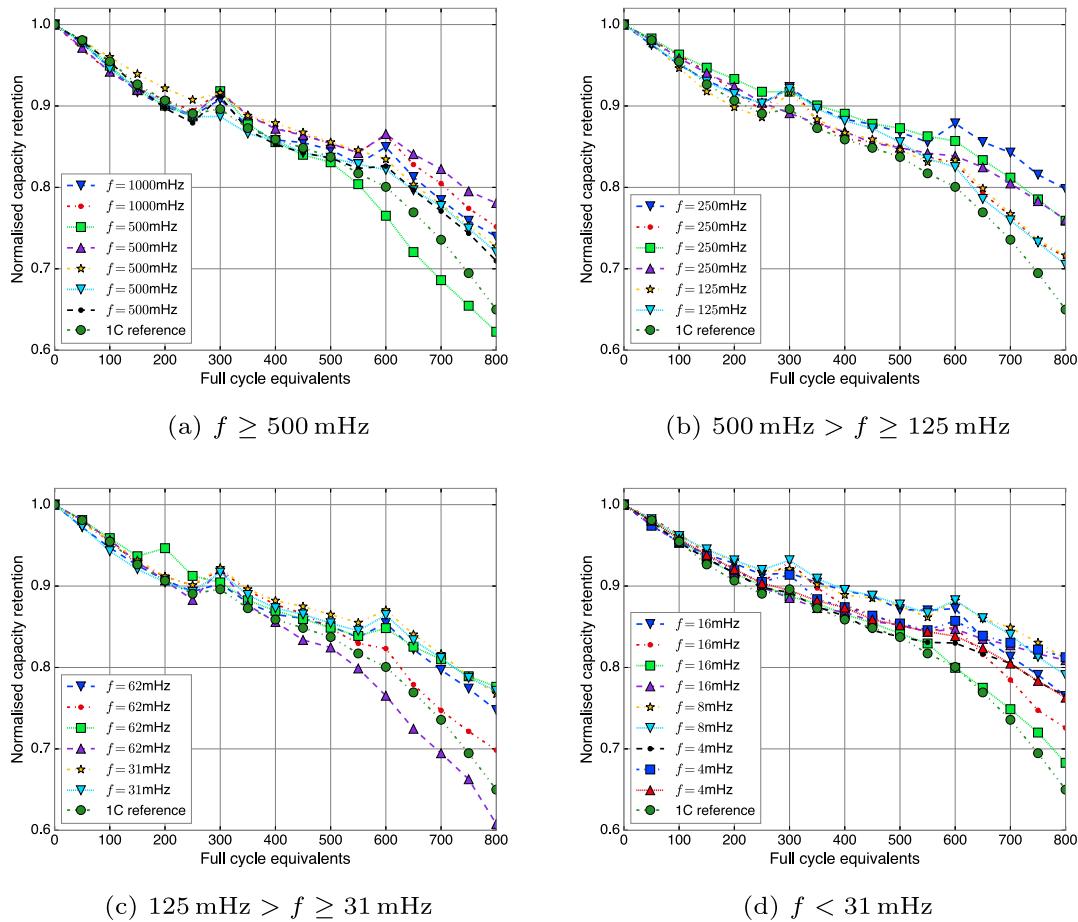
(a) $f \geq 500\,\mathrm{mHz}$

(b) $500\,\mathrm{mHz} > f \geq 125\,\mathrm{mHz}$

(c) $125\,\mathrm{mHz} > f \geq 31\,\mathrm{mHz}$

(d) $f < 31\,\mathrm{mHz}$

Fig. 3. Capacity fade plots for all tested cells, split into four subplots based on frequency, with decreasing frequency from top left to bottom right. All replicates performing the same test are shown in the same figure. Each subplot also include average of the three 1C reference test for comparison.

3.1. Comparison with 1C reference

As 1C constant current discharge is a typical standard test in battery cycling studies, it is important to note that despite the large variance in the individual tests, durability is improved in all but one of the dynamic test cases when comparing to the average of the 1C reference tests, see Fig. 3. This trend is also confirmed when including the resistance increase in the analysis, see Fig. 4 where the 1C reference is displaying the fastest resistance increase as well as the fastest capacity decay when comparing with several different pulse test conditions.

The fact that even as ageing behaviour changes for different pulse discharge cases the dynamic cycling is always outperforming the 1C reference shows that accounting for dynamics in battery durability testing is a vital feature. Therefore test studies aiming to investigate cycle life of BEV batteries should take dynamic usage into account when designing tests. It also complements the findings of Keil and Jossen [17] which showed that including regenerative breaking pulses in cycling tests improved durability, where our results show analogous results for dynamic discharge as compared to static discharge.

The causes for this cannot be clearly stated based on the tests performed in this study, but one hypothesis could be that periodic rest reduces local phenomena such as lithiation unbalance or local potential drops due to equilibration during rest phases. Pulses have also been mentioned previously in literature as a way to reduce concentration polarisation and utilisation of active material [27], so further speculation could be that the distribution of Li in the active material is improved by pulsing the current compared to constant current. This could help reduce material stress and decrease for instance crack formation in the material, but to verify these hypotheses further post-mortem analysis would be needed.

3.2. Splitting the dataset

The trend that lifetime decreases with higher frequency mentioned in Section 3 is more clearly present for lower frequencies, where as in higher frequencies the trend seems to be much weaker, or even non-existent. This can be further analysed by splitting the dataset into two subsets, where higher frequency pulses ($f > 100\,\mathrm{mHz}$) are analysed separately from lower frequency pulses. The differences in trends can be seen more clearly from Fig. 6 where the linear trends for the subsets of data are shown together with the test data from the study. The slope is large for the low frequency pulses, but more or less flat for the higher frequency.

The reasons for choosing $f = 100\,\mathrm{mHz}$ as the cut-off frequency is two-fold. Firstly it can be seen from the ageing data that it is around this frequency that the trends start diverging. Secondly, based on EIS sweeps on cells, the characteristic frequency for the charge transfer resistance and the double layer capacitance is between $100\,\mathrm{mHz}$ and $10\,\mathrm{Hz}$ and tending towards lower frequency as the cells age, see Fig. 7. Combining these two observations, one hypothesis can be that for frequencies higher than $f \approx 100\,\mathrm{mHz}$ the influence of the pulsation is dampened by passing the current through the double layer capacitance. This will cause charging and discharging of double layer capacitance during pulsing, which will lead to the effective concentration in the particles not being significantly different in the different frequency cases. Previous research on pulse current in LiBs have not focused on this, but previous research on lead–acid battery technology have linked the influence of double layer to performance [28,29]. This hypothesis would however require further study to draw more reliable conclusions.
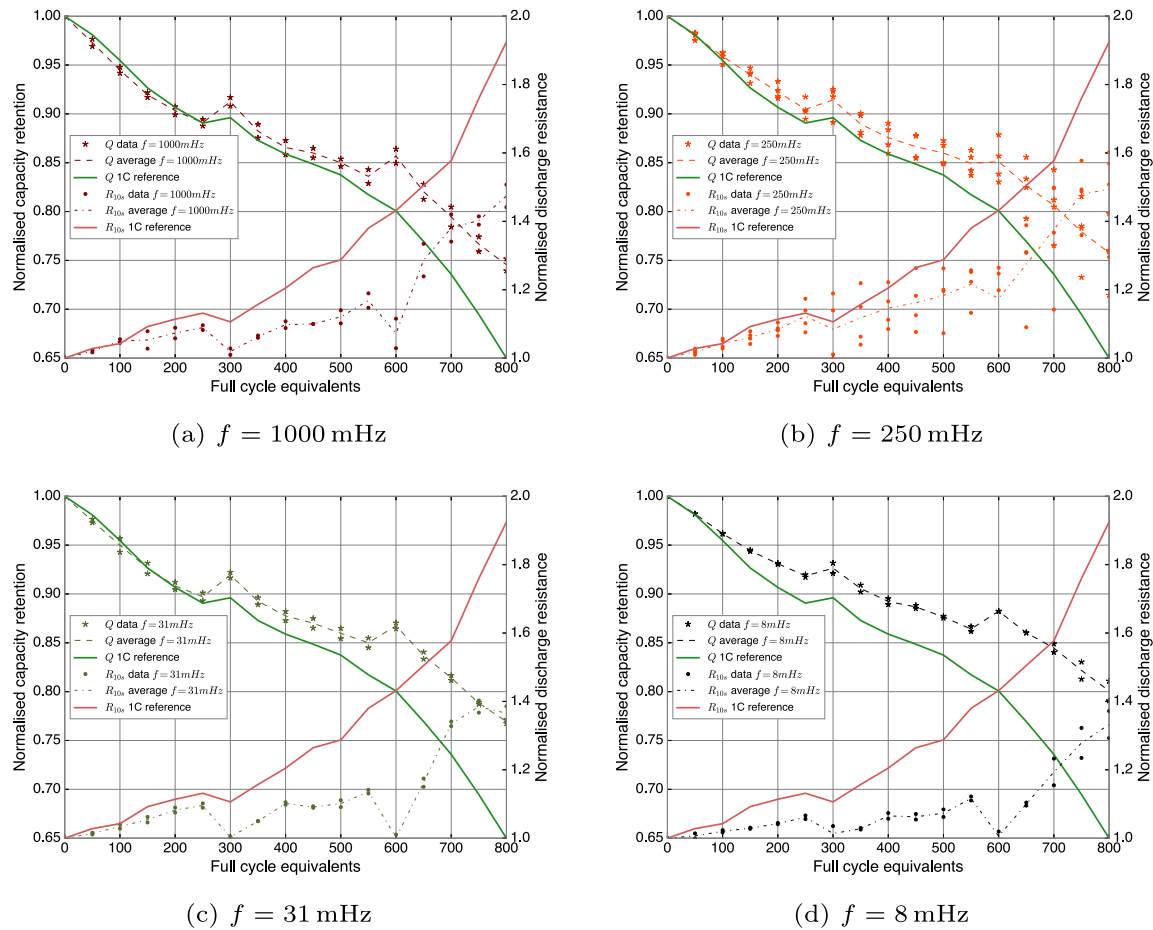
(a) $f = 1000\,\text{mHz}$

(b) $f = 250\,\text{mHz}$

(c) $f = 31\,\text{mHz}$

(d) $f = 8\,\text{mHz}$

Fig. 4. Average capacity fade and resistance increase for four cases of pulsed discharge plotted as dashed lines with the average capacity fade and resistance increase for 1C case as reference, plotted with solid lines. In all cases the pulsed discharge tests are showing better durability compared to 1C.
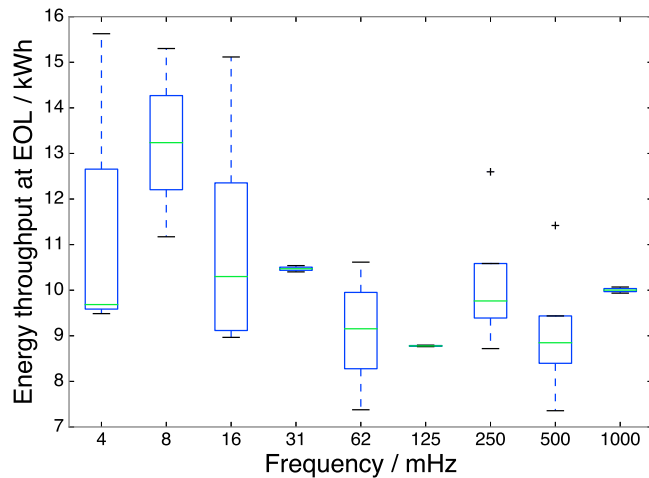

Fig. 5. Box plot of energy throughput at end of life for all test data grouped by pulse frequency. Large variance in the data can be noted for six out of nine test conditions, indicating surprisingly large spread in cell ageing performance.

Fig. 6. Pulse frequency versus energy throughput at end of life for all tests conducted in study, together with linear fits of end of life versus frequency for the two subsets of data.

3.3. ANOVA test on datasets

Even though the trends for the split datasets might look significantly different from direct inspection, the large variance in the test results means that there is a risk of misinterpreting pure variance as a trend. To verify that this is not the case further statistical analysis is performed on
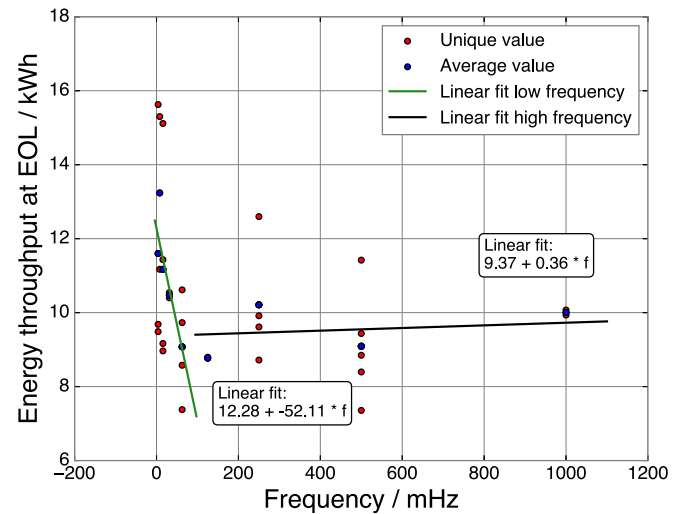
the datasets by applying the ANalysis Of VAriance (ANOVA) test. The ANOVA test, used here as implemented in the R software [30], finds with what probability a trend in results can be attributed to natural variance within the sample set. The null hypothesis being that the variations in results are indeed caused by variance and the means of
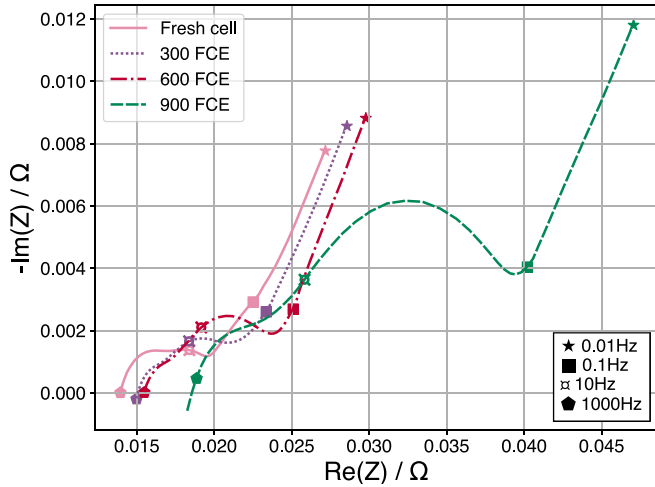
Fig. 7. Nyquist plot of EIS sweep after 0, 300, 600 and 900 FCE respectively. Markers on curve denote certain frequencies in the sweep, and it can be noted that the characteristic frequency is getting lower throughout testing.

Fig. 8. Differential voltage for full cell at beginning of life, and each electrode at beginning of life. Two capacities are marked between horizontal lines on the plot to indicate the capacity until central graphite peak, and between the two visible NCA peaks. Q_1 serves as a proxy for estimating the capacity loss of the Si-Gr, and Q_2 serves as proxy for estimating the capacity loss of NCA.

all individual tests are the same, generating a utility test of

$$H_0 : \mu_1 = \mu_2 = \cdots = \mu_i \text{ versus } H_1 : \mu_u \neq \mu_v \text{ for some } (u, v).$$

Based on the probability of rejecting H_0, the presence of a trend in the data is assessed, with $P(H_0) < 0.05$ used as condition for a statistically significant trend.

Examining the full dataset without a split by frequency the probability of null hypothesis is $P(H_0) = 0.28$ meaning that the null hypothesis can be rejected with only 72% probability. This result cannot be considered significant with the standard requirement, so the variations in means is considered attributed to variance rather than trend.

However if the data is split by frequency it becomes clear that the trend is present in the low frequency region, as $P(H_0) = 0.028$ for tests with $f < 100$ mHz indicating that the null hypothesis can be rejected with 97.2% probability, which can be considered a statistically significant trend. Conversely, analysis of the data where $f > 100$ mHz yields that $P(H_0) = 0.81$, or null hypothesis can only be rejected with 19% probability, and accordingly no relation can be established. This further enforces the observation that at lower frequency the pulse duration has an influence on the ageing of the battery, but at higher frequency the effect is negligible. These observations are also align with the findings in previous studies of Bessman et al. [20].

3.4. Negative electrode decay

To track the individual electrode ageing without intrusive testing, the differential voltage curve of the full cell is recreated by a combination of positive and negative electrode voltage curves, see Fig. 8. Details on the half-cell implementation is found in 2.3. The capacity of the coin cells used for half cell characterisation needs to be scaled to full cell, and electrode balancing taken into account. Following the method proposed in Mussa et al. [31] the scaled electrode capacities, $Q_{neg/pos}$ are formulated as

$$Q_{neg} = s_{neg}q_{neg} + \sigma_{neg} \tag{1}$$

$$Q_{pos} = s_{pos}q_{pos} + \sigma_{pos} \tag{2}$$

with $q_{neg/pos}$ denoting the capacity measured in the coin cell, $s_{neg/pos}$ and $\sigma_{neg/pos}$ denoting the scale and slip factor respectively. Using the scaled capacities together with the voltage curves measured, allows the approximation of full cell voltage as the difference between the
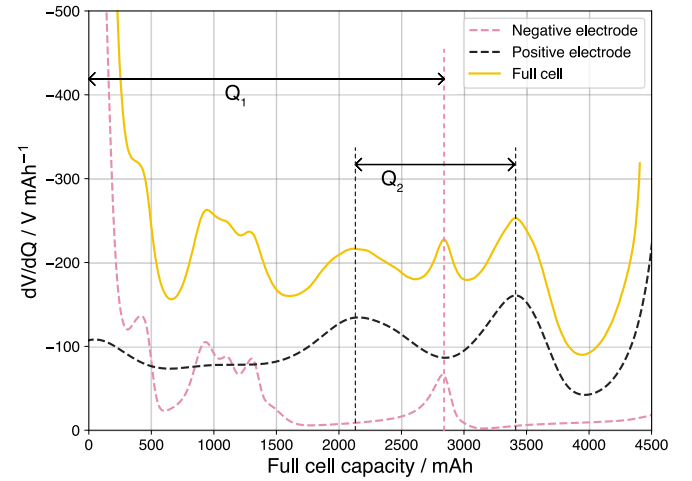
electrode potentials, $U_{cell} = U_{pos} - U_{neg}$ with $U_{neg/pos} = f(Q_{neg/pos})$ based on measured voltage on half cells.
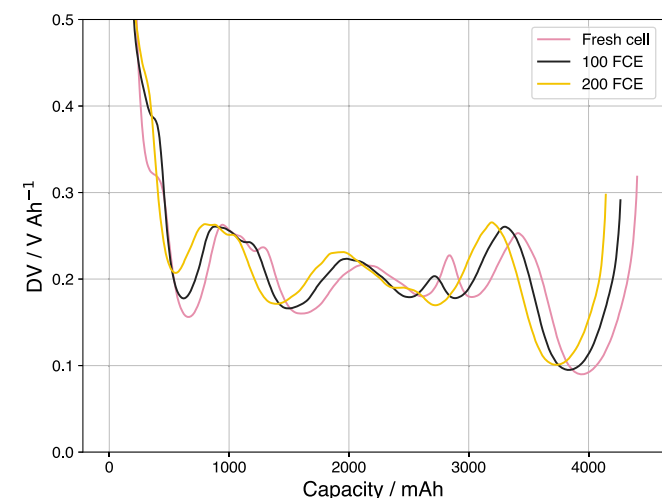
By calculating the derivative of voltage with respect to capacity, dV/dQ, of these curves a Differential Voltage Analysis (DVA) can be performed. Overlaying the DVA curves from the half cells and the full cell, the peaks can be clearly assigned to a unique electrode, see Fig. 8. This allows one to define proxies to track the capacity of the individual electrodes by tracking the distance in capacity between DVA peaks.

Following the method presented by Zülke et al. in [32] the distance between the peaks associated to each electrode, the relative capacity of the electrodes can be tracked. For NCA the capacity defined as Q_2 in Fig. 8 indicates the capacity available between the two phase shifts. Analogously for the Si-Gr electrode, the capacity, defined as Q_1, until the central graphite peak appears, is taken as a proxy of the electrode capacity. This which however has an inherent weakness in not being able to distinguish between loss of active material and loss of lithium inventory due to only being referenced to one peak. The reason for using only one peak can be deduced from Fig. 9(a) which shows how the relative slip of the electrodes makes the peaks associated with the negative electrode around 30% SOC and 65% SOC non-identifiable as degradation progresses.
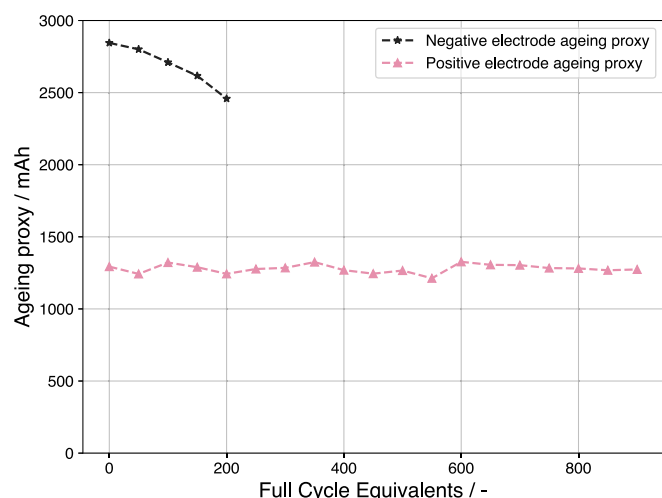
These values can then be tracked throughout the ageing testing to indicate the individual ageing of each electrode, and the result is shown in Fig. 9(b). Due to peaks shifting in the DVA with ageing, the central graphite peak becomes indistinguishable, and unfortunately this means that Q_1 cannot be calculated beyond 200 FCE. Yet the trend is clear from the data that can be obtained, showing that the negative electrode capacity is dropping swiftly, whereas the positive electrode capacity can be considered more or less unchanged throughout the test, with the fluctuations stemming from the noise of the measurement data.

This trend can be further investigated by the novel method of analysing the difference between charge and discharge voltage of ICA tests, as shown in Fig. 10(a). The difference is defined simply as $\Delta U = U_{chrg} - U_{dchg}$ for the same point in SOC.

For the ICA test, that is performed with a c-rate of $C/20$ it can be assumed that overpotentials in the cell are low, and thus the difference between charge and discharge can be attributed to hysteresis effects mainly. Silicon electrodes are known to show significant voltage hysteresis [33,34], so a large difference between charge and discharge in the low SOC region, is an indicator of Si in the composite electrode. Furthermore, as the resistance in the cell increases with ageing, see
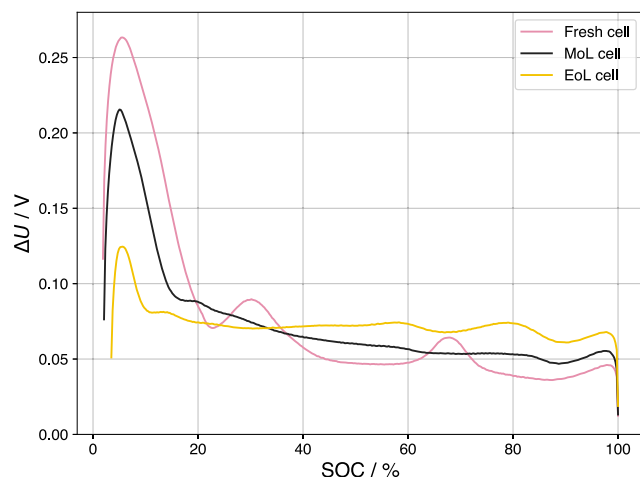
(a) Differential Voltage plot.

(a) Voltage hysteresis.

(b) Ageing proxies for negative and positive electrode.

(b) Incremental Capacity plot with peaks associated with Si marked.

Fig. 10. Voltage hysteresis (a) and Incremental Capacity plot (b) for the same cell at three stages of ageing. Both figures indicate near complete loss of active Si when cell is at end of life (EoL).
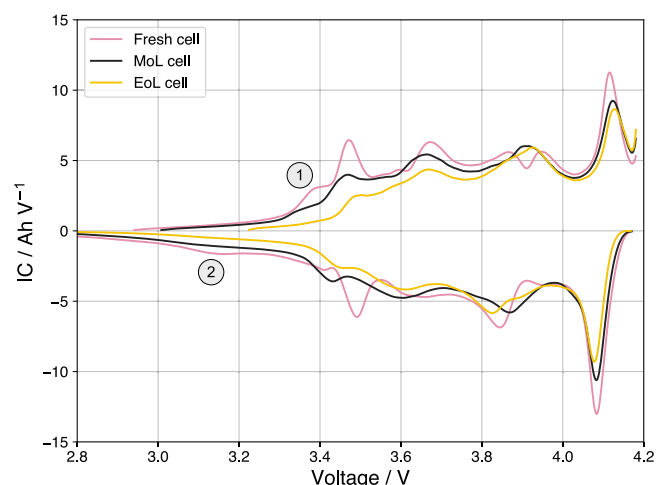
Fig. 9. Disappearance of distinct DVA peak for negative electrode capacity (a) and the ageing proxies for positive and negative electrode respectively (b).

Fig. 4, any overpotential contribution to ΔU will increase with ageing, yielding the expected trend that ΔU would increase if there are no changes in the underlying OCP curves. It is however clear from the data that ΔU is decreasing in the lower SOC region, which is a clear indication that Si is being lost at a disproportionate rate during cycling. This aligns with the previous findings in literature that Si composites can have issues with cycle life, mainly due to large volumetric changes during charge and discharge [35–37].

The hypothesis that Si capacity loss is the main contributor to the initial negative electrode capacity loss is further corroborated with analysis of the Incremental Capacity Analysis (ICA) sweeps. ICA is the inverse derivate compared to DVA as dQ/dV such that valleys in the DVA show up as peaks in ICA. ICA sweeps performed during life testing is shown in Fig. 10(b), where the peaks associated with Si for low voltages, are quickly diminishing. As the cell reaches its end of life the peaks are completely gone, indicating that there is very little active silicon remaining in the negative electrode.

3.5. Future work

Several interesting questions arise from the findings in this paper that would be interesting to investigate further. More detailed post-mortem analysis to further investigate the different ageing mechanisms involved and finding a more detailed physical explanation to why the degradation is faster in constant current cycling compared to dynamic cycling. Coin cell harvesting at end of life to be able to improve the results from voltage fitting shown in Section 3.4 would also be of value to further elucidate the internal processes.

4. Conclusion

After splitting the data it can be concluded that the investigated discharge harmonics does not have significant influence on ageing performance in higher frequencies, but there is a statistically significant trend in the region where $f < 100\,\text{mHz}$. In this region, the energy throughput that the cells manage before reaching end of life increases with decreasing frequency. This indicates that slower dynamic loads would be beneficial for battery life compared to fast dynamic loads.

The reasons for this trend need to be investigated further, but a hypothesis for higher frequency is proposed, with the effect of higher frequency being smoothened out by double layer capacitance charge and discharge during cycling.

All tests performed with some form of dynamic load, outperform the standard 1C test performed for reference, which showed the poorest durability performance of all tests. This indicates that standard static tests are not fully representative for the dynamic use case that is experienced in real life applications, and for assessing durability performance test protocols that include dynamic usage should be considered.

Further findings indicate that the degradation of the cells are mainly due to capacity loss on the negative electrode side, and more specifically on the Si part of Si-Gr composite electrode. Previous studies suggest that this is due to volumetric expansion causing breakage of the SEI layer, and the lack of stable SEI layer causes rapid ageing. This trend is similar for all tested cells and show no discernible dependence on frequency.

CRediT authorship contribution statement

Kristian Frenander: Conceptualization, Methodology, Writing – original draft, Writing – review & editing, Visualization. **Torbjörn Thiringer:** Conceptualization, Writing – review & editing, Supervision, Funding acquisition, Project administration, Resources.

Declaration of competing interest

The authors declare the following financial interests/personal relationships which may be considered as potential competing interests: Kristian Frenander reports financial support and administrative support were provided by Volvo Car Corporation.

Data availability

Data will be made available on request.

Acknowledgements

References

[1] J.R. Szczech, S. Jin, Nanostructured silicon for high capacity lithium battery anodes, Energy Environ. Sci. 4 (1) (2011) 56–72, http://dx.doi.org/10.1039/c0ee00281j.

[2] X. Li, A.M. Colclasure, D.P. Finegan, D. Ren, Y. Shi, X. Feng, L. Cao, Y. Yang, K. Smith, Degradation mechanisms of high capacity 18650 cells containing Si-graphite anode and nickel-rich NMC cathode, Electrochim. Acta 297 (2019) 1109–1120, http://dx.doi.org/10.1016/j.electacta.2018.11.194.

[3] M.N. Obrovac, L. Christensen, Structural changes in silicon anodes during lithium insertion/extraction, Electrochem. Solid-State Lett. 7 (5) (2004) http://dx.doi.org/10.1149/1.1652421.

[4] M.N. Obrovac, V.L. Chevrier, Alloy negative electrodes for Li-ion batteries, Chem. Rev. 114 (23) (2014) 11444–11502, http://dx.doi.org/10.1021/cr500207g.

[5] J.M. Tarascon, M. Armand, Issues and challenges facing rechargeable lithium batteries, in: Materials for Sustainable Energy: A Collection of Peer-Reviewed Research and Review Articles from Nature Publishing Group, World Scientific Publishing Co., 2010, pp. 171–179, http://dx.doi.org/10.1142/9789814317665_0024.

[6] C.K. Chan, H. Peng, G. Liu, K. McIlwrath, X.F. Zhang, R.A. Huggins, Y. Cui, High-performance lithium battery anodes using silicon nanowires, Nature Nanotechnol. 3 (1) (2008) 31–35, http://dx.doi.org/10.1038/nnano.2007.411, URL www.nature.com/naturenanotechnology.

[7] J.Y. Li, Q. Xu, G. Li, Y.X. Yin, L.J. Wan, Y.G. Guo, Research progress regarding Si-based anode materials towards practical application in high energy density Li-ion batteries, Mater. Chem. Front. 1 (9) (2017) 1691–1708, http://dx.doi.org/10.1039/c6qm00302h, URL https://pubs.rsc.org/en/content/articlehtml/2017/qm/c6qm00302h.

[8] X. Zuo, J. Zhu, P. Müller-Buschbaum, Y.J. Cheng, Silicon based lithium-ion battery anodes: A chronicle perspective review, Nano Energy 31 (2017) 113–143, http://dx.doi.org/10.1016/j.nanoen.2016.11.013.

[9] C. Liu, K. Qian, D. Lei, B. Li, F. Kang, Y.B. He, Deterioration mechanism of LiNi0.8Co0.15Al0.05O2/graphite-SiO:X power batteries under high temperature and discharge cycling conditions, J. Mater. Chem. A 6 (1) (2017) 65–72, http://dx.doi.org/10.1039/c7ta08703a, URL https://pubs.rsc.org/en/content/articlehtml/2018/ta/c7ta08703a.

[10] P. Teichert, G.G. Eshetu, H. Jahnke, E. Figgemeier, Degradation and aging routes of ni-rich cathode based li-ion batteries, Batteries 6 (1) (2020) 1–26, http://dx.doi.org/10.3390/batteries6010008.

[11] F. Farmakis, I. de Meatza, T. Subburaj, D. Tsiplakides, D.P. Argyropoulos, S. Balomenou, I. Landa-Medrano, A. Eguia-Barrio, N. Strataki, M. Nestoridi, Elucidation of the influence of operating temperature in LiNi0.8Co0.15Al0.05O2/silicon and LiNi0.8Co0.15Al0.05O2/graphite pouch cells batteries cycle-life degradation, J. Energy Storage 41 (2021) 102989, http://dx.doi.org/10.1016/j.est.2021.102989.

[12] J. Schmitt, M. Schindler, A. Jossen, Change in the half-cell open-circuit potential curves of silicon–graphite and nickel-rich lithium nickel manganese cobalt oxide during cycle aging, J. Power Sources 506 (July) (2021) 230240, http://dx.doi.org/10.1016/j.jpowsour.2021.230240.

[13] E. Moyassari, T. Roth, S. Kücher, C.-C. Chang, S.-C. Hou, F.B. Spingler, A. Jossen, The role of silicon in silicon-graphite composite electrodes regarding specific capacity, cycle stability, and expansion, J. Electrochem. Soc. 169 (1) (2022) 010504, http://dx.doi.org/10.1149/1945-7111/ac4545.

[14] I. Zilberman, J. Sturm, A. Jossen, Reversible self-discharge and calendar aging of 18650 nickel-rich, silicon-graphite lithium-ion cells, J. Power Sources 425 (2019) 217–226, http://dx.doi.org/10.1016/j.jpowsour.2019.03.109.

[15] I. Profatilova, E. De Vito, S. Genies, C. Vincens, E. Gutel, O. Fanget, A. Martin, M. Chandesris, M. Tulodziecki, W. Porcher, Impact of silicon/graphite composite electrode porosity on the cycle life of 18650 lithium-ion cell, ACS Appl. Energy Mater. 3 (12) (2020) 11873–11885, http://dx.doi.org/10.1021/acsaem.0c01999.

[16] G. Baure, M. Dubarry, Synthetic vs. Real driving cycles: A comparison of electric vehicle battery degradation, Batteries 5 (2) (2019) 42, http://dx.doi.org/10.3390/batteries5020042.

[17] P. Keil, A. Jossen, Impact of dynamic driving loads and regenerative braking on the aging of lithium-ion batteries in electric vehicles, J. Electrochem. Soc. 164 (13) (2017) A3081–A3092, http://dx.doi.org/10.1149/2.0801713jes.

[18] J. Schmalstieg, S. Käbitz, M. Ecker, D.U. Sauer, A holistic aging model for Li(NiMnCo)O2 based 18650 lithium-ion batteries, J. Power Sources 257 (2014) 325–334, http://dx.doi.org/10.1016/j.jpowsour.2014.02.012.

[19] S.B. Peterson, J. Apt, J.F. Whitacre, Lithium-ion battery cell degradation resulting from realistic vehicle and vehicle-to-grid utilization, J. Power Sources 195 (8) (2010) 2385–2392, http://dx.doi.org/10.1016/j.jpowsour.2009.10.010.

[20] A. Bessman, R. Soares, O. Wallmark, P. Svens, G. Lindbergh, Aging effects of AC harmonics on lithium-ion cells, J. Energy Storage 21 (2019) 741–749, http://dx.doi.org/10.1016/j.est.2018.12.016.

[21] M.J. Lacey, Influence of the electrolyte on the internal resistance of lithium sulfur batteries studied with an intermittent current interruption method, ChemElectroChem 4 (8) (2017) 1997–2004, http://dx.doi.org/10.1002/celc.201700129.

[22] K. Rumpf, A. Rheinfeld, M. Schindler, J. Keil, T. Schua, A. Jossen, Influence of cell-to-cell variations on the inhomogeneity of lithium-ion battery modules, J. Electrochem. Soc. 165 (11) (2018) A2587–A2607, http://dx.doi.org/10.1149/2.0111811jes.

[23] S.F. Schuster, M.J. Brand, P. Berg, M. Gleissenberger, A. Jossen, Lithium-ion cell-to-cell variation during battery electric vehicle operation, J. Power Sources 297 (2015) 242–251, http://dx.doi.org/10.1016/j.jpowsour.2015.08.001.

[24] B. Epding, B. Rumberg, H. Jahnke, I. Stradtmann, A. Kwade, Investigation of significant capacity recovery effects due to long rest periods during high current cyclic aging tests in automotive lithium ion cells and their influence on lifetime, J. Energy Storage 22 (December 2018) (2019) 249–256, http://dx.doi.org/10.1016/j.est.2019.02.015.

[25] M. Lewerenz, G. Fuchs, L. Becker, D.U. Sauer, Irreversible calendar aging and quantification of the reversible capacity loss caused by anode overhang, J. Energy Storage 18 (2018) 149–159, http://dx.doi.org/10.1016/j.est.2018.04.029.

[26] J. Wilhelm, S. Seidlmayer, P. Keil, J. Schuster, A. Kriele, R. Gilles, A. Jossen, Cycling capacity recovery effect: A coulombic efficiency and post-mortem study, J. Power Sources 365 (2017) 327–338, http://dx.doi.org/10.1016/j.jpowsour.2017.08.090, URL https://www.sciencedirect.com/science/article/pii/S0378775317311230.

[27] F. Savoye, P. Venet, M. Millet, J. Groot, Impact of periodic current pulses on Li-ion battery performance, IEEE Trans. Ind. Electron. 59 (9) (2011) 3481–3488.

[28] A. Kirchev, M. Perrin, E. Lemaire, F. Karoui, F. Mattera, Studies of the pulse charge of lead-acid batteries for PV applications: Part I. Factors influencing the mechanism of the pulse charge of the positive plate, J. Power Sources 177 (1) (2008) 217–225.

[29] A. Kirchev, F. Mattera, E. Lemaire, K. Dong, Studies of the pulse charge of lead-acid batteries for photovoltaic applications: Part IV. Pulse charge of the negative plate, J. Power Sources 191 (1) (2009) 82–90.

[30] J.M. Chambers, A.E. Freeny, R.M. Heiberger, Analysis of variance; designed experiments, in: Statistical Models in S, Routledge, 2018, pp. 145–193, http://dx.doi.org/10.1201/9780203738535-5.

[31] A.S. Mussa, M. Klett, M. Behm, G. Lindbergh, R.W. Lindström, Fast-charging to a partial state of charge in lithium-ion batteries: A comparative ageing study, J. Energy Storage 13 (2017) 325–333, http://dx.doi.org/10.1016/j.est.2017.07.004.

[32] A. Zülke, Y. Li, P. Keil, R. Burrell, S. Belaisch, M. Nagarathinam, M.P. Mercer, H.E. Hoster, High-energy nickel-cobalt-aluminium oxide (NCA) cells on idle: Anode-versus cathode-driven side reactions, Batteries & Supercaps 4 (6) (2021) 934–947, http://dx.doi.org/10.1002/batt.202100046, URL https://onlinelibrary.wiley.com/doi/full/10.1002/batt.202100046.

[33] N. Ding, J. Xu, Y.X. Yao, G. Wegner, X. Fang, C.H. Chen, I. Lieberwirth, Determination of the diffusion coefficient of lithium ions in nano-Si, Solid State Ion. 180 (2–3) (2009) 222–225, http://dx.doi.org/10.1016/j.ssi.2008.12.015.

[34] B. Lu, Y. Song, Q. Zhang, J. Pan, Y.T. Cheng, J. Zhang, Voltage hysteresis of lithium ion batteries caused by mechanical stress, Phys. Chem. Chem. Phys. 18 (6) (2016) 4721–4727, http://dx.doi.org/10.1039/C5CP06179B, URL https://pubs.rsc.org/en/content/articlehtml/2016/cp/c5cp06179b.

[35] M. Ashuri, Q. He, L.L. Shaw, Silicon as a potential anode material for Li-ion batteries: where size, geometry and structure matter, Nanoscale 8 (1) (2016) 74, http://dx.doi.org/10.1039/c5nr05116a.

[36] M. Winter, J.O. Besenhard, M.E. Spahr, P. Novak, Insertion electrode materials for rechargeable lithium batteries, Adv. Mater. 10 (10) (1998) 725–763, http://dx.doi.org/10.1002/(SICI)1521-4095(199807)10:10.

[37] E. Moyassari, L. Streck, N. Paul, M. Trunk, R. Neagu, C.-C. Chang, S.-C. Hou, B. Märkisch, R. Gilles, A. Jossen, Impact of silicon content within silicon-graphite anodes on performance and Li concentration profiles of li-ion cells using neutron depth profiling, J. Electrochem. Soc. 168 (2) (2021) 020519, http://dx.doi.org/10.1149/1945-7111/abe1db, URL https://iopscience.iop.org/article/10.1149/1945-7111/abe1db.